JOURNAL OF SOLID STATE CHEMISTRY 44, 326–336 (1982)

Investigations of the Tin–Antimony–Oxygen System by High-Resolution Electron Microscopy

DAVID J. SMITH

High Resolution Electron Microscope, University of Cambridge, Free School Lane, Cambridge, CB2 3RQ, U.K.

L. A. BURSILL

School of Physics, University of Melbourne, Parkville, Victoria, 3052, Australia

AND FRANK J. BERRY

Department of Chemistry, University of Birmingham, P.O. 363, Birmingham, B15 2TT, U.K.

Received May 10, 1982

A range of tin–antimony oxides, prepared by the calcination of precipitates, were examined by high-resolution electron microscopy. Products formed at 600°C contain small crystals of a rutile-type material and, depending on antimony concentration, varying amounts of disordered and/or amorphous phases. The observations are consistent with a resistivity to bulk phase equilibrium under conditions of low temperature and high antimony concentrations. Heating of the tin–antimony oxides to 1000°C for prolonged periods is accompanied by an increase in the crystallinity and particle size of the rutile-type material as a result of the thermally induced aggregation of tin(IV) oxide units. The observations are consistent with limited antimony incorporation in the bulk tin(IV) oxide lattice and a migration of antimony to surface sites. There was no evidence for any discrete, readily identifiable, antimony oxide phases, although a nonrutile-type material was observed at higher antimony concentration. The rutile-type phases often contained planar faults which were identified in some instances as twin boundaries; the possibility that these might provide a means of accommodating antimony within the tin oxide lattice is briefly considered. The relationship between our observations and the information available from other techniques is discussed.

Introduction

Despite their commercial development as catalysts (*1*), surprisingly few details of the fundamental structural properties of tin–antimony oxides formed by the calcination of precipitates have been established. Although recent investigations of these materials by X-ray diffraction (*2, 3*) and electron microscopy (*3*) have been restricted by their poor crystallinity and small particle size, the X-ray diffraction data (*2, 3*) have revealed the limited solubility of antimony in tin(IV) oxide and ESCA (*4, 5*) has shown the thermally induced enrichment of the surface with antimony. Furthermore, Mossbauer spectroscopy (*6–8*) has shown the apparent accommodation of antimony(V) in the bulk tin(IV) oxide lattice and antimony(III) at the surface. Although

0022-4596/82/120326-11$02.00/0

electron microscopy at low resolution of tin–antimony oxides formed by calcination of precipitates (*3*) and of vapor-phase-deposited crystals (*9*) has found evidence for twinned microcrystals, the defect structure and the nature of the surface layers of these materials remains obscure (*2, 3*).

High-resolution electron microscopy is capable of elucidating localized irregularities and surface phenomena down to the atomic level and may therefore reveal microstructural detail which has hitherto been too fine to resolve. We report here on some observations of a range of tin–antimony oxides of differing compositions, following calcination at various temperatures, with a high-resolution electron microscope (HREM) (*10, 11*) having a directly interpretable image resolution approaching 2 Å (*12*). Such electron-optical performance provides the capacity to discern structural defects at the atomic level and to identify crystalline phases directly from the fringe spacings and geometry, even for particles smaller than 20 Å in diameter (*13*). In a subsequent paper (*14*), we shall relate further observations on other similar materials to their catalytic properties.

Experimental

The tin–antimony oxides were prepared by the simultaneous addition of the required proportions of antimony(V) chloride and tin(IV) chloride to ammonium hydroxide solution. The white precipitates were filtered, washed with water, dried at 120°C, and calcined at 600°C for 16 hr; most samples were then subjected to further calcination as described in Table I. Samples suitable for electron microscopy were prepared by gently grinding the material in an agate pestle and mortar under ethanol, and allowing a drop of the resulting suspension to dry on a holey carbon film.

High-resolution observations were carried out with the Cambridge University 600-kV HREM (*10, 11*), operated at an accelerating voltage of 500 kV. Magnifications for image recording were typically in the region of 200,000–300,000 times although magnifications as high as 800,000 were com-

TABLE I

TIN–ANTIMONY OXIDES: DETAILS OF CALCINATION AND SUMMARY OF OBSERVATIONS

Sample	Percentage antimony	Calcination	Observations
A	2	600°C/16 hr/air	Small SnO_2 crystals, some twinned; considerable disorder/defects.
B	4	600°C/16 hr/air; 1000°C/17 days/air	Medium SnO_2 crystals, some twinned; disordered/faulted crystals; some amorphous phase.
C	10	600°C/16 hr/air; 600°C/14 days/sealed tube	Very small SnO_2 crystals; much amorphous material.
D	10	600°C/16 hr/air; 1000°C/13 days/air	Medium SnO_2 crystals, more twins; less disorder, amorphous layer on SnO_2 crystals.
E	20	600°C/16 hr/air	Very small SnO_2 crystals; much amorphous material.
F	20	600°C/16 hr/air; 1000°C/14 days/air	Large SnO_2 crystals, often twinned; considerable disorder and amorphous surface layer; very large nonrutile crystals, beam-sensitive.
G	40	600°C/16 hr/air; 1000°C/14 days/air	Large SnO_2 crystals, often twinned; very large nonrutile-type crystals; amorphous/crystalline "conglomerates."

monly used for the initial correction of image astigmatism. Observations were restricted, whenever possible, to crystal areas projecting over holes in the support film in order to avoid overlap interference in the image arising from the support. A standard optical bench, equipped with a 10-mW He–Ne laser, was normally used to provide quick and accurate measurement of the lattice spacings recorded in the high-resolution image.

Results

The electron microscope observations are briefly summarized in Table I.

Tin–Antimony Oxide A

The material consisted primarily of small crystals, with diameters of ca. 100–800 Å, often containing planar faults, which were identified in some instances as twin boundaries. In some regions, there was also considerable disorder and a high density of crystalline defects. A typical low-magnification image is shown in Fig. 1a. Electron diffraction patterns consisted of rings characteristic of rutile-type tin(IV) oxide (Fig. 1b) with the strongest reflections corresponding to the 3.35 (110), 2.64 (101), 2.34 (200), and 1.76-Å (211) lattice spacings. No evidence was found in either the high-resolution images or the diffraction patterns for any nonrutile-type crystalline or amorphous phase.

Tin–Antimony Oxide B

This sample was polycrystalline with particle diameters ranging between ca. 500 and 3000 Å. A typical field of view, together with an electron diffraction pattern, is shown in Fig. 2. The most prominent rings of the diffraction pattern again correspond to the (110), (101), (200), and (211) reflections of tin(IV) oxide; their sharpness, relative to those of Fig. 1b, reflects the in-

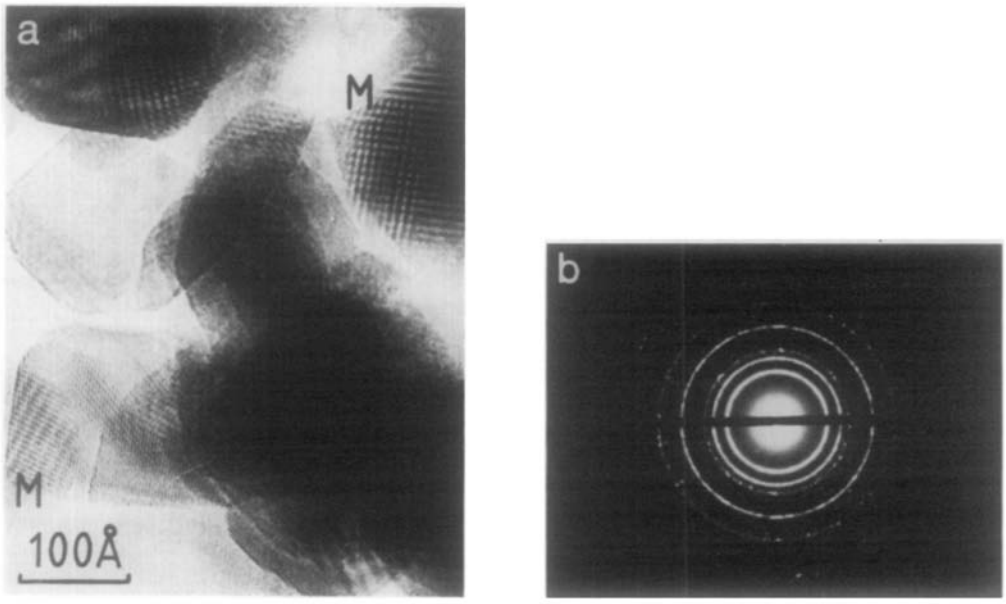

FIG. 1. (a) Image of tin–antimony oxide A showing typical particle morphology—the coarse fringes (M) are due to moiré effects from overlapping crystals. (b) Corresponding electron diffraction pattern confirming the polycrystalline nature of the sample and the small particle size. Ring diameters correspond to tin(IV) oxide lattice spacings only.

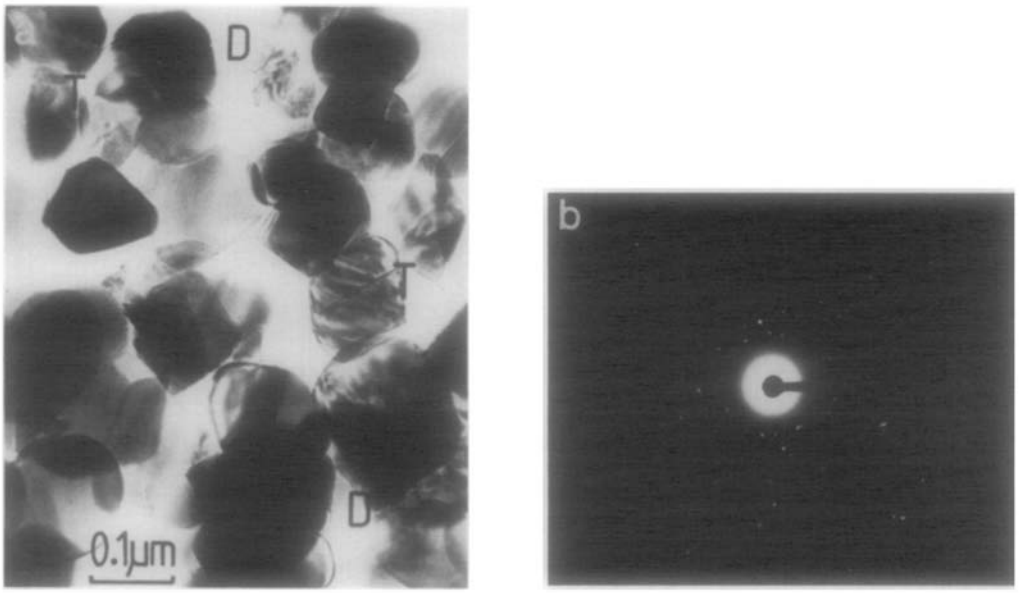

FIG. 2. (a) Low-magnification image of tin–antimony oxide B: twins (T) and regions of disorder (D) are marked. (b) Electron diffraction pattern for sample B.

creased crystal size. No evidence was found for the presence of any antimony oxide.

Detailed examination revealed that a substantial fraction of these particles contained planar faults. Although the particle size distribution precluded tilting of the support grid to bring the principal axes of a crystal parallel to the incident beam, accurate orientations were achieved in some cases by chance enabling some of these faults to be identified as twin boundaries. Figure 3, for example, shows a well-defined example of such a fault which was readily identified from the lattice–fringe spacings and geometry as a (101)-type twin boundary. It is also interesting to note the nearby region of disordered planar faults shown in Fig. 4.

With a slightly defocused objective lens, and diffraction contrast (i.e., small objective aperture), many other crystals were located which were close to a diffracting condition for at least one set of reflections; these crystals were subsequently identified from the lattice fringes present in high-magnification, high-resolution images. Figure 5, for example, shows an extended perfect crystal of tin(IV) oxide containing a set of 2.64-Å (101) lattice fringes.

Although no antimony oxide was detected in this sample heated to 1000°C for a

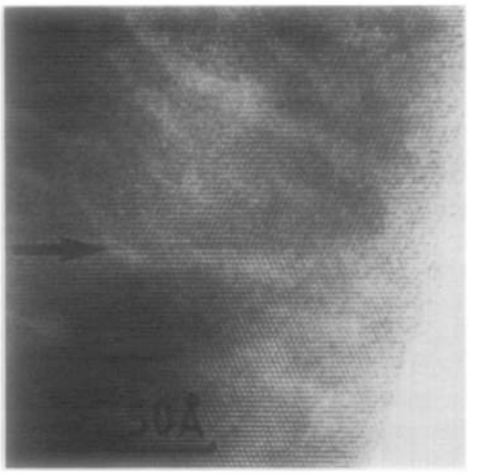

FIG. 3. High-resolution image (sample B) showing a (101)-type twin boundary (arrow) in a large SnO_2 crystal.

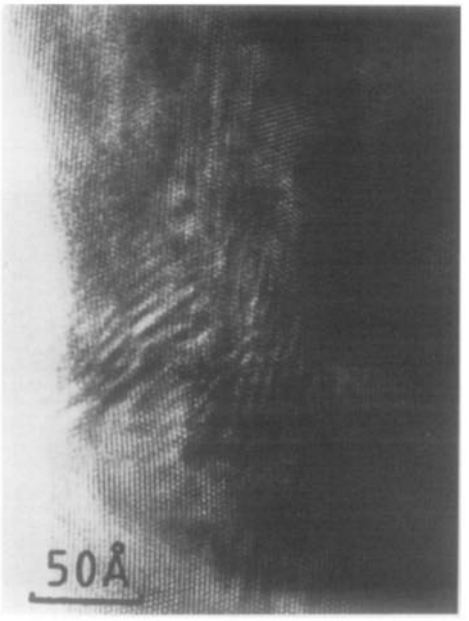

FIG. 4. Region of extended planar faults near boundary shown in Fig. 3.

prolonged period, it is significant that many of the crystalline regions observed, such as those in Fig. 6, showed extensive disorder with many faults and defects clearly visible. We also observed some regions of almost complete disorder, as well as areas of amorphous material having no apparent crystallinity except for the odd microcrystallite (Fig. 7).

Tin–Antimony Oxide C

The material was composed predominantly of very small randomly oriented crystallites with diameters in the range 30–120 Å, and dispersed throughout an apparently amorphous phase (Fig. 8). The polycrystalline nature of the material gave rise to broad diffuse rings in the electron diffraction pattern which were consistent with reflections corresponding to the lattice spacings of tin(IV) oxide. Although the microcrystals generally appeared to be perfect, often with sharp, well-defined edges (Fig. 9a), some defective crystals were also

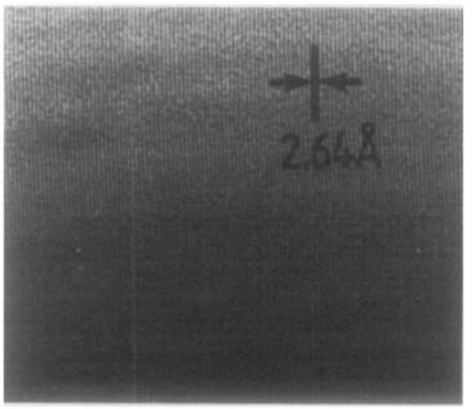

FIG. 5. Extended perfect crystal of SnO_2 from sample B with strong one-dimensional lattice fringes of 2.64-Å spacing.

observed (Fig. 9b). Several different lattice spacings could be measured from high-magnification images of these microcrystallites. The most prevalent were the 3.35- (110) and 2.64-Å (101) lattices of tin dioxide. Diffraction patterns recorded on the optical bench also indicated further spacings of 2.35 (common) and 1.76 Å (occasional), which correspond to the SnO_2 (200) and (211) re-

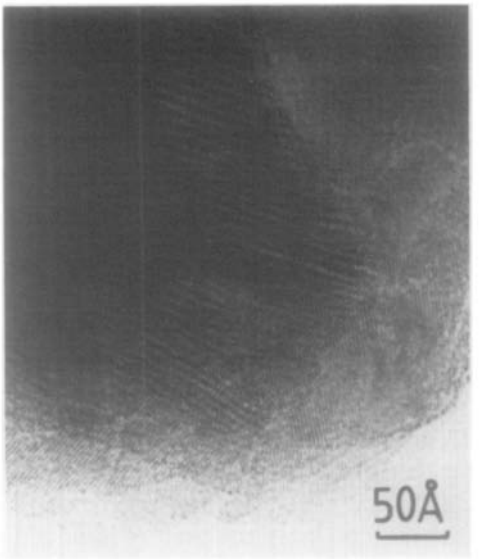

FIG. 6. Region of extensive disorder from sample B.

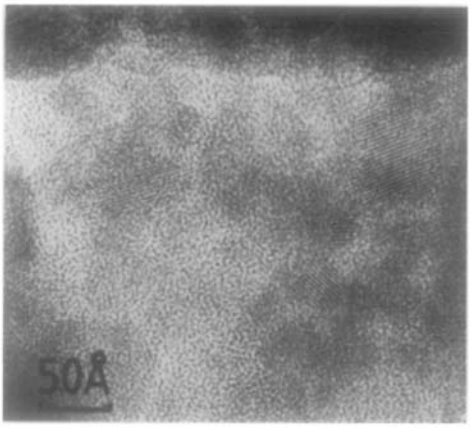

FIG. 7. Region of predominantly amorphous material from sample B containing some SnO_2 microcrystallites.

flections. No evidence of a crystalline antimony oxide phase was observed.

Tin–Antimony Oxide D

This material showed the presence of a crystalline rutile-type phase similar to that previously observed in the sample containing 4% antimony which had also been heated to 1000°C (sample B). However, comparison of the two materials showed that this oxide with a higher nominal antimony concentration exhibited a substantial increase in the number of crystals which appeared to be twinned and a decrease in the amount of disordered material. Furthermore, amorphous layers were observed on the surfaces of the rutile-type crystals in addition to more general regions of amorphous material throughout the sample. Figure 10a illustrates a typical specimen region which may be compared with Fig. 2a. The electron diffraction pattern (Fig. 10b) consisted of sharp rings peaked at the major SnO_2 lattice spacings and, significantly, gave no evidence for the presence of any discrete antimony tetroxide.

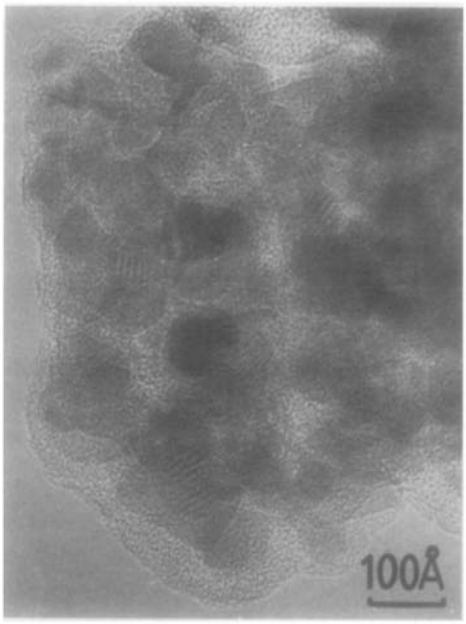

FIG. 8. Low-magnification image of tin–antimony oxide C showing microcrystallites of tin(IV) oxide dispersed throughout an amorphous phase.

Tin–Antimony Oxide E

Electron microscopy revealed crystal sizes (ca. 30–100 Å; Fig. 11a) smaller than those observed in the material containing 2% antimony and calcined at 600°C for 16 hr (sample A). Electron diffraction patterns (Fig. 11b) showed the characteristic broad rings, consistent with the small crystal size,

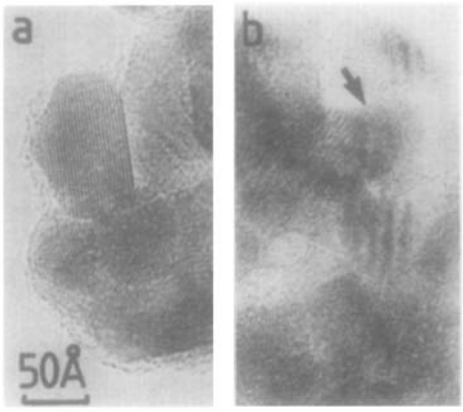

FIG. 9. (a) Small microcrystallite from sample C with sharp, well-defined edge. (b) Region of sample C showing small, apparently defective, microcrystallite (arrow).

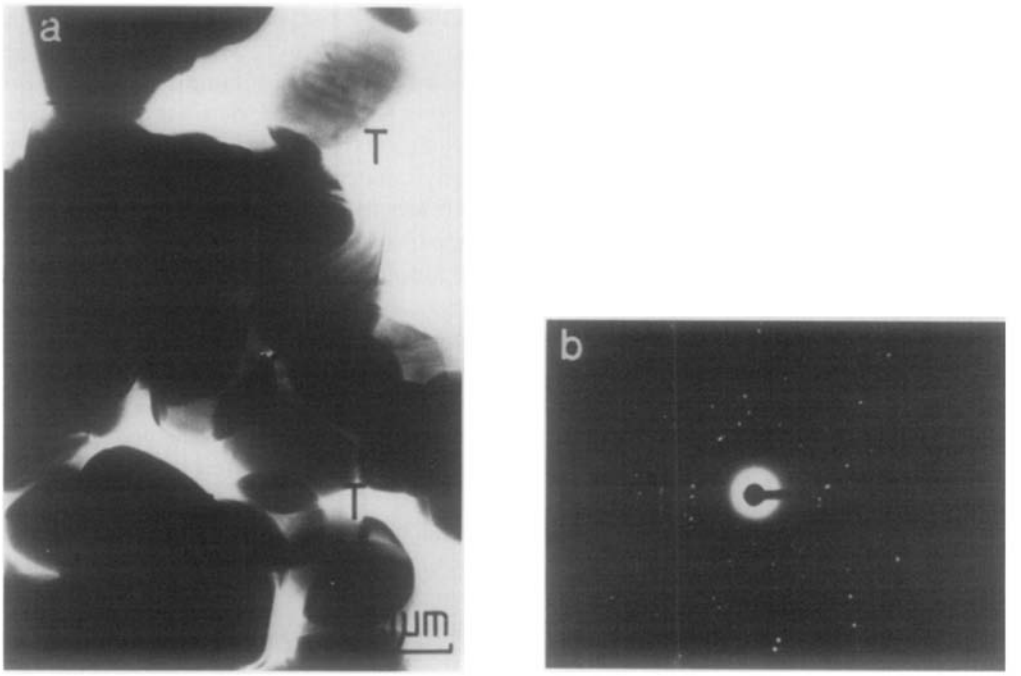

FIG. 10. (a) Typical region of tin–antimony oxide D showing a number of twinned crystals marked T. (b) Electron diffraction pattern from sample D.

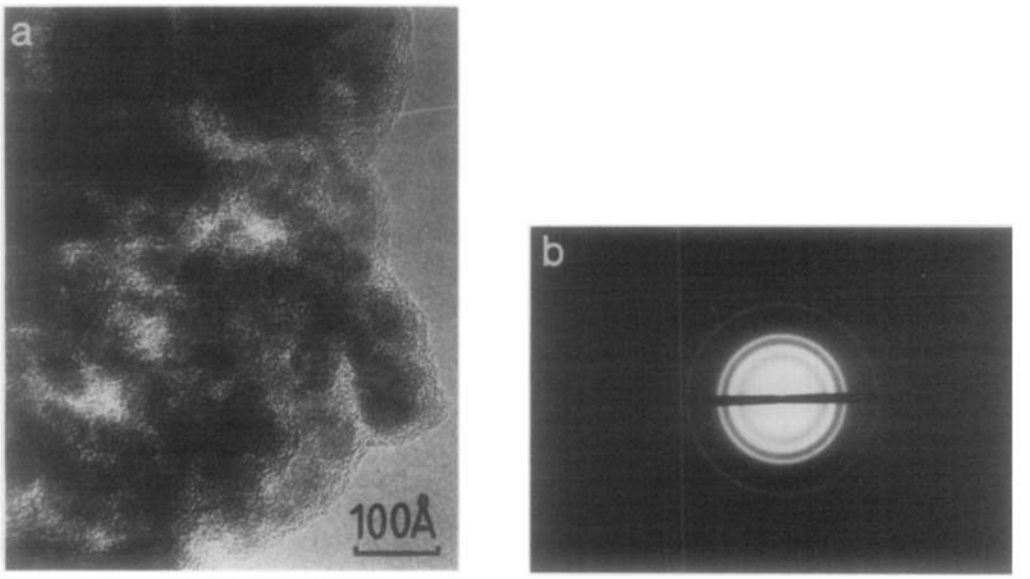

FIG. 11. (a) Low-magnification image of tin–antimony oxide E showing amorphous material and microcrystallites of tin(IV) oxide. (b) Electron diffraction pattern from sample E—the broad diffuse rings (cf. Figs. 1b and 2b) reflect the very small particle size.

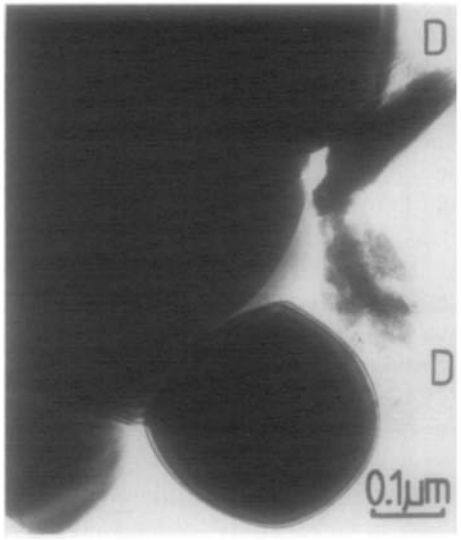

FIG. 12. Low-magnification image of tin–antimony oxide F—regions of disorder (marked D) remain despite higher calcination treatment.

with spacings again corresponding to tin(IV) oxide. Substantial amounts of amorphous material in the regions surrounding these small, often faceted, crystals were also observed.

Tin–Antimony Oxide F

Calcination of sample F containing 20% antimony for 14 days at 1000°C showed the development of large crystals (ca. 3000 Å–1 μm) which were frequently twinned and which gave electron diffraction patterns characteristic of tin(IV) oxide. Smaller crystalline particles with less well-defined shape, but which were often twinned, were also seen. The sample showed small amounts of amorphous material with gross disorder (Fig. 12), as well as amorphous surface layers on the rutile-type crystals.

We also observed very large crystals (typically several microns) which electron diffraction established to be of a nonrutile-type structure. These crystals proved to be sensitive to the electron beam: with high current densities at the specimen (several A/cm^2), beam damage in the form of localized defects was observed. These beam-sensitive crystals, whose crystal structure is not yet determined, are to be the subject of further investigation.

Tin–Antimony Oxide G

This material showed evidence of three phases: large, extensively twinned crystals (ca. 2500–4000 Å) giving electron diffraction patterns characteristic of tin(IV) oxide; very large crystals of a nonrutile nature, similar to those observed in sample F; and, finally, an interesting phenomenon of some smaller crystals (ca. 1000–1500 Å) embedded in a disordered manner into larger crystals, often in the presence of some apparently amorphous material (Fig. 13).

Discussion

Effect of Calcination on the Formation of Tin–Antimony Oxides

The white precipitates formed by addition of antimony(V) and tin(IV) chlorides to ammonium hydroxide may be considered as amorphous gels containing Sn(IV) and Sb(V) in separate octahedral hydroxyl envi-

FIG. 13. Region of tin–antimony oxide G showing a number of small crystals apparently embedded in a large crystal.

ronments (*3, 8*). Heating to ca. 600°C for 16 hr is reported to produce poorly crystalline dehydrated solids (*3*) containing Sb(V) and Sn(IV) (*6*). The small, sometimes disordered, rutile-type crystalline material seen in samples A, C, and E suggest that low-temperature calcination fails to induce large-scale aggregation of tin(IV) oxide units. Moreover, a comparison of our observations for samples A and E shows that the primary effect of increased antimony content (from 2 to 20%) at 600°C is to cause a substantial decrease in the size of the rutile-type crystals and an increase in the amorphous content. It would appear that the amorphous material observed in the more antimony-rich solids contains antimony which, at low temperatures, inhibits the development of the crystalline rutile-type phase. Furthermore, heating for 14 days in a sealed tube (sample C) does *not* lead to increased crystallinity, even when the antimony concentration is quite low. This indicates the difficulty with which bulk equilibrium is achieved in the tin–antimony oxide system by low-temperature calcination. Finally, it is notable that we found no evidence for the formation of any separate antimony oxide phases.

The most significant observation from samples heated at 1000°C for long periods of time (samples B, D, F, and G) involves the enhanced crystallinity and increased particle sizes of the rutile-type phase. Moreover, despite prolonged thermolysis, it is interesting that all four samples exhibit regions of disorder and thereby provide further evidence for the resistivity of these materials to the attainment of bulk equilibrium. However, we are unable to confirm at present that some of this disorder does not arise from the cooling process. It is significant that, although no evidence was found in any of these materials heated at high temperatures for any identifiable antimony oxides, we observed crystals with a nonrutile-type structure in those samples with nominally high antimony content (samples F and G).

The material containing 4% antimony, heated to 1000°C (sample B), corresponds to the limit of antimony solubility in tin(IV) oxide (*3*). Although regions of disorder could be observed, the amorphous content of this material was far less pronounced than in any of the materials containing larger amounts of antimony; this is consistent with the incorporation of only low concentrations of antimony within the bulk tin(IV) oxide lattice. The larger concentrations of amorphous material in the other three samples heated at 1000°C suggest that the thermally induced enrichment of the surface by antimony (*4, 5*) leads to the formation of crystalline antimony tetroxide which, although volatilized at high temperatures, leaves a noncrystalline residual deposit containing antimony. However, we are unable to confirm the suggestion (*4*) that materials heated at similar temperatures, albeit for shorter periods of time, are solid solutions of antimony in tin(IV) oxide containing a discrete antimony tetroxide phase at the surface. Our results are compatible with an alternative model (*3, 5*) in which surface enrichment leads to the formation of antimony tetroxide which is volatilized at 1000°C to give a solid solution in which the antimony-enriched surface contains antimony atoms surrounded entirely by tin atoms in nearest-neighbor sites.

Comparison with Other Techniques

Our observations of the tin–antimony oxides, particularly those relating to the high-temperature calcination, are in reasonable agreement with the results of other indirect techniques applied to their characterization. For example, calcination at 1000°C is reported to correspond to a monophasic equilibrated rutile-type solid solution of ca. 4% antimony in tin(IV) oxide (*3*), which X-ray photoelectron spectroscopy shows to be enriched at the surface with up to 25%

antimony (*5*)—the enrichment reflecting the thermally induced migration of antimony from the bulk of the rutile-type phase. It seems from ESCA data (*4*) that volatile Sb_2O_4 is formed only at surface antimony compositions greater than ca. 25% and that bulk compositions with less than 4% antimony generate surface compositions at 1000°C which are below the critical value. Indeed, it appears that only those oxides containing less than 4% antimony fail to produce biphasic material composed of rutile and Sb_2O_4 phases when heated at high temperatures for prolonged periods. The deficit of amorphous surface material observed here in the material containing 4% antimony (sample B) reflects this phenomenon. Moreover, it should also be noted that our results indicate the presence of the Sb_2O_4 phase as an amorphous layer spread over the surface of the rutile-type material, rather than in the form of discrete crystals.

Role of High-Resolution Electron Microscopy

While morphological details of the tin–antimony oxides can be inferred from essentially bulk techniques such as X-ray diffraction, the utilization of high-resolution electron microscopy in the characterization of these materials has provided unique information at the direct lattice level, as well as confirmation, or otherwise, of some of the inferences of the bulk methods. Hence the existence of the amorphous surface layers (samples D and F), the coexistence of microcrystallites of tin(IV) oxide with an amorphous phase (samples B, C, E, and G), and the occurrence of substantial twinning in the tin oxide crystals, and of considerable disorder, have all been established here by direct observation. High-resolution electron microscopy should thus prove invaluable for the structural investigation of related materials, particularly in monitoring structural changes which take place during catalysis.

Twin Boundaries

While twinning is most often associated with either growth or deformation faults in crystals, it is also a means by which cations may enjoy an environment other than that provided by the bulk material: twinning can therefore be a means of accommodating impurities (*15*). It is significant therefore that in studies of pure and antimony-doped SnO_2 (*9*), twinning was only observed in the latter material: it was suggested that the twinning could be considered as a means whereby antimony could be accommodated within the tin(IV) oxide lattice. Indeed, two plausible models for the boundary incorporating the antimony were proposed, although it was recognized that no experimental evidence for the location of the antimony relative to the twin planes had been obtained. It is relevant here to mention that a recent neutron diffraction study of a mixed antimony–tin oxide has led to a proposed model structure based on the occupation by Sb(III) of interstitial sites within the tin(IV) oxide rutile-type lattice (*16*). Furthermore, recent computed-image simulations of a {011} glide twin boundary have given excellent agreement with an equivalent experimental series of images of a boundary in an antimony-doped tin(IV) oxide crystal *without* requiring the presence of any antimony (*17*). In the present study, all materials heated to 1000°C (samples B, D, F, and G), together with the material containing 2% antimony and heated to 600°C for 16 hr, appear to have planar faults, some of which we identified as twin boundaries. It would therefore appear that twinning is not necessarily confined to materials calcined at high temperatures. While it is tempting and plausible to suggest that these represent a site for most of the incorporated antimony, such a model is not justified in the light of the studies mentioned above. It would seem that microanalysis both at and away from some of these

boundaries is needed to resolve this question.

Acknowledgments

The Cambridge University 600-kV High Resolution Electron Microscope was built as a joint project between the Cavendish Laboratory and the Department of Engineering with major financial support from the Science Research Council: continued support of the HREM Project is gratefully acknowledged.

References

1. D. J. HUCKNALL, "Selective Oxidation of Hydrocarbons," p. 42, Academic Press, New York/London, 1974.
2. J.-L. PORTEFAIX, P. BUSSIERE, M. FORISSIER, F. FIGUERAS, J. M. FRIEDT, J. P. SANCHEZ, AND F. THEOBALD, *J. Chem. Soc. Faraday I* **76**, 1652 (1980).
3. D. R. PYKE, R. REID, AND R. J. D. TILLEY, *J. Chem. Soc. Faraday I* **76**, 1174 (1980).
4. Y. BOUDEVILLE, F. FIGUERAS, M. FORISSIER, J.-L. PORTEFAIX, AND J. C. VEDRINE, *J. Catal.* **58**, 52 (1979).
5. Y. M. CROSS AND D. R. PYKE, *J. Catal.* **58**, 61 (1979).
6. F. J. BERRY, P. E. HOLBOURN, AND F. W. D. WOODHAMS, *J. Chem. Soc. Dalton*, 2241 (1980).
7. F. J. BERRY AND B. J. LAUNDY, *J. Chem. Soc. Dalton*, 1442 (1981).
8. F. J. BERRY, *J. Catal.* **73**, 349 (1982).
9. D. R. PYKE, R. REID, AND R. J. D. TILLEY, *J. Solid State Chem.* **25**, 231 (1978).
10. W. C. NIXON, H. AHMED, C. J. D. CATTO, J. R. A. CLEAVER, K. C. A. SMITH, A. E. TIMBS, P. W. TURNER, AND P. M. ROSS, "Electron Microscopy and Analysis 1977," (D. L. Misell, Ed.), p. 13, Institute of Physics, Bristol and London, 1977.
11. V. E. COSSLETT, *Proc. Roy. Soc. London Ser. A* **370**, 1 (1980).
12. V. E. COSSLETT, R. A. CAMPS, W. O. SAXTON, D. J. SMITH, W. C. NIXON, H. AHMED, C. J. D. CATTO, J. R. A. CLEAVER, K. C. A. SMITH, A. E. TIMBS, P. W. TURNER, AND P. M. ROSS, *Nature (London)* **281**, 49 (1979).
13. D. J. SMITH, R. M. FISHER, AND L. A. FREEMAN, *J. Catal.* **72**, 51 (1981).
14. F. J. BERRY AND D. J. SMITH, in preparation.
15. S. ANDERSSON AND B. G. HYDE, *J. Solid State Chem.* **9**, 92 (1974).
16. F. J. BERRY AND C. GREAVES, *J. Chem. Soc. Dalton*, 2447 (1981).
17. L. A. BURSILL, G. J. WOOD, AND D. J. SMITH, in preparation.